shock factor 1 (HSF-1) transcription factor rapidly induces the expression of heat shock proteins (HSPs) [2] involved in the refolding or clearance of heat-damaged proteins [3]. In addition to such cell-autonomous responses, the activation of stress responses in the nervous system helps to integrate external and internal cues across tissues to regain homeostasis; this is the case for heat shock and other stresses [4,5].

Neurons are crucial in regulating many physiological processes cell nonautonomously, including systemic accumulation of fat and the rebalance of energy. Across species, there are many well-established examples of neuronal circuits, involving a variety of neurotransmitters and neurohormonal signals, which modulate fat metabolism [6±9]. In *C. elegans*, many neurohormonal signals converge on the regulation of fat stores in the gut by controlling either the expression of catabolic lipases [10] or of fat desaturases involved in de novo fatty acid (FA) synthesis [11±13]. Notably, the transforming growth factor û/bone morphogenetic protein (TGF- /BMP) signaling pathway provides a good example of this regulation. DBL-1 is the *C. elegans* sole TGF- /BMP ligand, homologous to vertebrate BMP10 [14,15]. DBL-1 is secreted from neuronal cells to control body size, reproductive output, and fat stores [12]. Both the environmental triggers that control the release of neurohormonal signals, such as DBL-1, and the adaptive value of this form of regulation remain unexplored.

In this study, neuronal overexpression of *hsf-1* (*hsf-1*^{neuro}) was used as a tool to study the systemic consequences of neuronal *hsf-1* activation. We found that *hsf-1*^{neuro} decreased the expression of fat desaturases *fat-6/fat-7*Ð orthologues of the human stearoyl-CoA desaturaseÐ while activating the expression of catabolic lysosomal lipases, with consequent depletion of fat stores in the intestine. We find that the quantity and composition of phosphatidylinositol (PI) and phosphatidylethanolamine (PE)Ð phospholipids that make the bulk of the plasma membraneÐ are changed, and a notable shift in the saturation levels of the FA composition of the

Results

Overexpression of ***hsf-1*** in neurons leads to a cumulative adaptive advantage at warmer temperatures, and it is sufficient to fine-tune desaturation of glycerophospholipids (PLs)

Several pieces of evidence indicate that HSF-1 functions to retard the aging process. First, *hsf-1* knockdown

WT animals raised at warm temperatures and ***hsf-1^{neuro}*** raised at lower temperatures share a common transcriptional fat remodeling program

If *hsf-1^{neuro}* animals were constitutively acclimated to warmer temperatures, then they should share at least some of the transcriptional responses that animals mount in response to growth at 25ÊC. To explore this point, we identified differentially expressed (DE) genes between *hsf-1^{neuro}* (20ÊC) and wt (20ÊC) by DEseq2 (see Methods) and found 2,136 DE genes (S3 Table). These data were compared to DE genes from published sources that compared the transcriptomes of wt animals grown at 15ÊC with animals grown at 25ÊC [29]. Using different filtering criteria, we observed an overlap significantly higher than expected by chance (S4 Table). The Venn diagram in Fig 2A shows that the 2 sets of DE genes overlap by about 10%. Fig 2B shows the gene ontology (GO) categories of the overlapping genes, including lysosomal lipases required for lipid degradation (highlighted in Fig 2C). *C. elegans* contain at least 5 lysosomal lipases, LIPL-1 to LIPL-5 [30,31]. Some lipases are activated by the acidic environment of the lysosome to break down lipid droplets (LDs) and recycle FAs back into the cytosol, where they can be broken down by -oxidation or recycled into membranes [32]. We observed that the transcripts encoding *lipl-1/2/3* and *lipl-5* are up-regulated in *hsf-1^{neuro}* compared to WT animals raised at the same temperature (20ÊC) (Fig 2D).

LIPL-1 and LIPL-3 belong to the family of adipocyte triglyc Td (same)Tpared982 dtoto

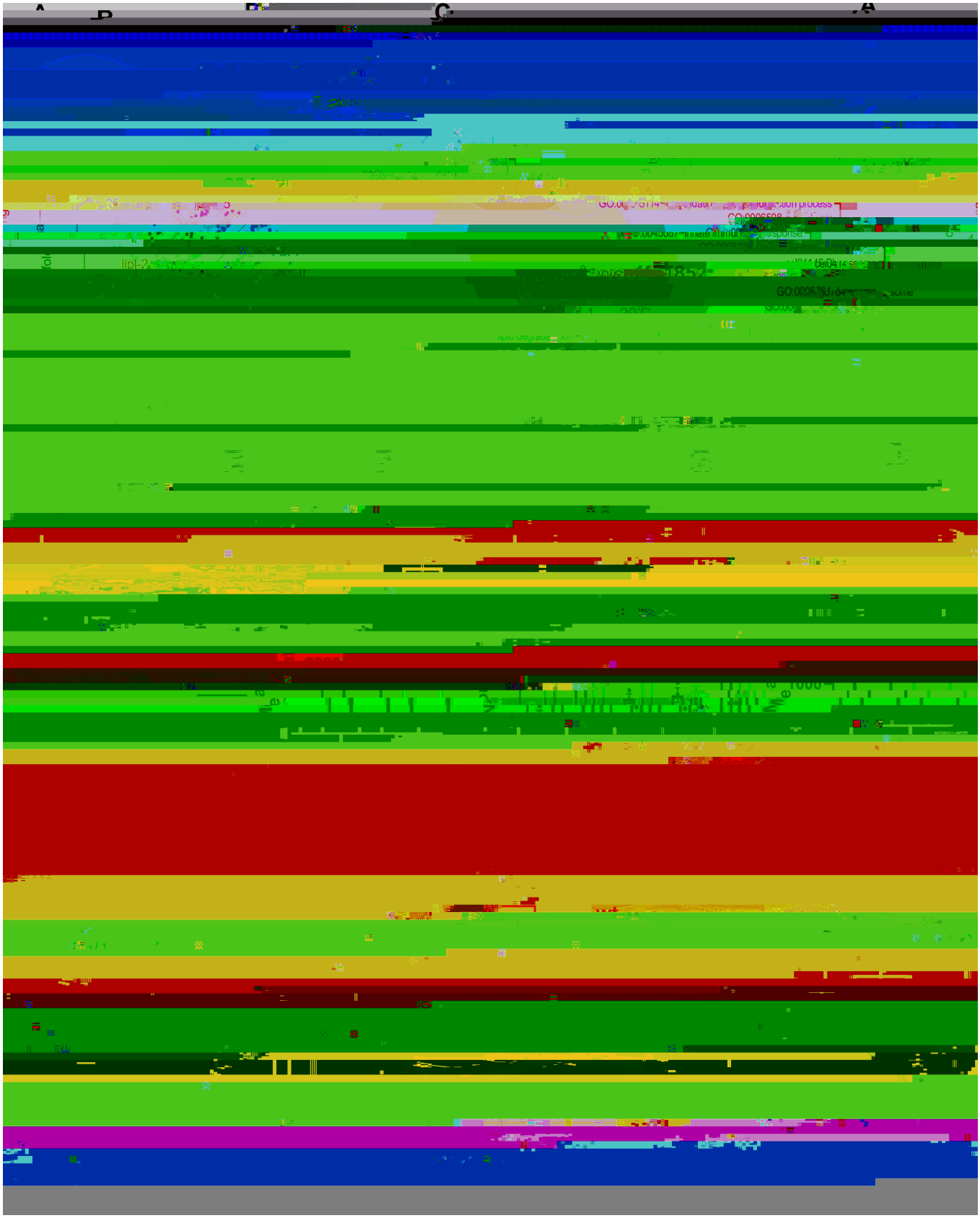

in *hsf-1*^{neuro} nematodes relative to wt (S1A and S1B Fig), ruling out starvation or an altered feeding behavior as explanatory mechanisms.

If activity of the lipases was increased, then their primary catabolic target, lipid stores, should be reduced. *C. elegans* do not have dedicated adipocytes instead storing fats in organelles called LDs in the intestine and hypodermis [32]. LDs are quantified using the lipid-intercalating fluorescent dye BODIPY [38]. We observed a reduction in BODIPY fluorescence of 29.3% in *hsf-1*^{neuro} *#1* and 40% in *hsf-1*^{neuro} *#2*, relative to wt young adult animals (Fig 2E±2G). Together, this evidence further confirms that a catabolic program activated by *hsf-1*^{neuro} alters FA storage and distribution.

The fat desaturases FAT-6 and FAT-7 produce oleic acid (OA), which is an important component of LDs [19], and, therefore, a reduced activity may also contribute to decreased fat storages. *Fat-7* is also key to homeoviscous adaptation, and it is transcriptionally down-regulated in animals raised at 25ÊC compared to those raised at 15ÊC (Fig 2C) [19]. To study the effect of *hsf-1*^{neuro} in vivo, we used a transcriptional *fat-7* reporter [39]. We find the fluorescent output of this reporter to be decreased in the 2 *hsf-1*^{neuro} lines by 28.7% in *hsf-1*^{neuro} *#1* and by 38.9% in*hsf-1*^{neuro} *#2* relative to wt (Fig 2H and 2I). Similarly, an in vivo reporter of *fat-6* is decreased by 51% in *hsf-1*^{neuro} *#2* worms compared to age-matched control animals (Fig 2J). If the observed decrease in the transcriptional output of these enzymes in *hsf-1*^{neuro} [illegible] accompanied by a concomitant reduction of their enzymatic output, a reduction in OA levels is to be expected. To /F8 1 T01 210.213imp21.03185 1 Tf (7e83 0 Td72behavior)287 0 Td 3dye

stores, de novo synthesis of unsaturated FA, and production and saturation of membrane phospholipids, are altered in *hsf-1*^{neuro} animals.

TAX-2/TAX-4 cGMP channels are essential for the fat remodeling phenotype caused by ectopic activation of neuronal stress

In *hsf-1*^{neuro} animals, *hsf-1* is expressed under the *rab-3* promoter that directs expression exclusively in all head neurons. To dissect the specific neurons that are responsible for the non±cell autonomous effect of *hsf-1*^{neuro} on fat metabolism, we first narrowed down neuronal classes by performing a suppressor RNAi screen. We selected 7 candidates based on their previously identified role on sensory neuron development or activity (Methods). As expected, when animals carrying an extrachromosomal array of *hsf-1*^{neuro} (*Exhsf-1*^{neuro}) were fed with an empty vector (EV), there is a significant 37% reduction in the transcriptional output of the *fat-7p*::*GFP* compared to their wt siblings (S6 Table). We found that among the RNAi treatments, the loss of *tax*-2 caused the strongest suppression of the effect of extrachromosomal neuronal overexpression of *hsf-1* (Ex *hsf-1*^{neuro}) on *fat-7* expression (Fig 3A). TAX-2 and TAX-4 are the and subunits, respectively, of a heterodimeric cGMP gated cation channel that is required for the proper function of several sensory neurons linked to chemosensation, thermotaxis, and Dauer formation [40,41].

Tax-4 RNAi had only a slight effect on *hsf-1*^{neuro}, and the difference with *tax-2* RNAi could be due to incomplete KD by the RNAi treatment, so we tested a loss-of-function (Lof) allele in the TAX-4 subunit. We find that *tax-4(p678)*, which causes dysfunction in all 12 TAX-2/4± expressing neurons [42], shows slightly higher levels of expression than controls; however, the difference does not

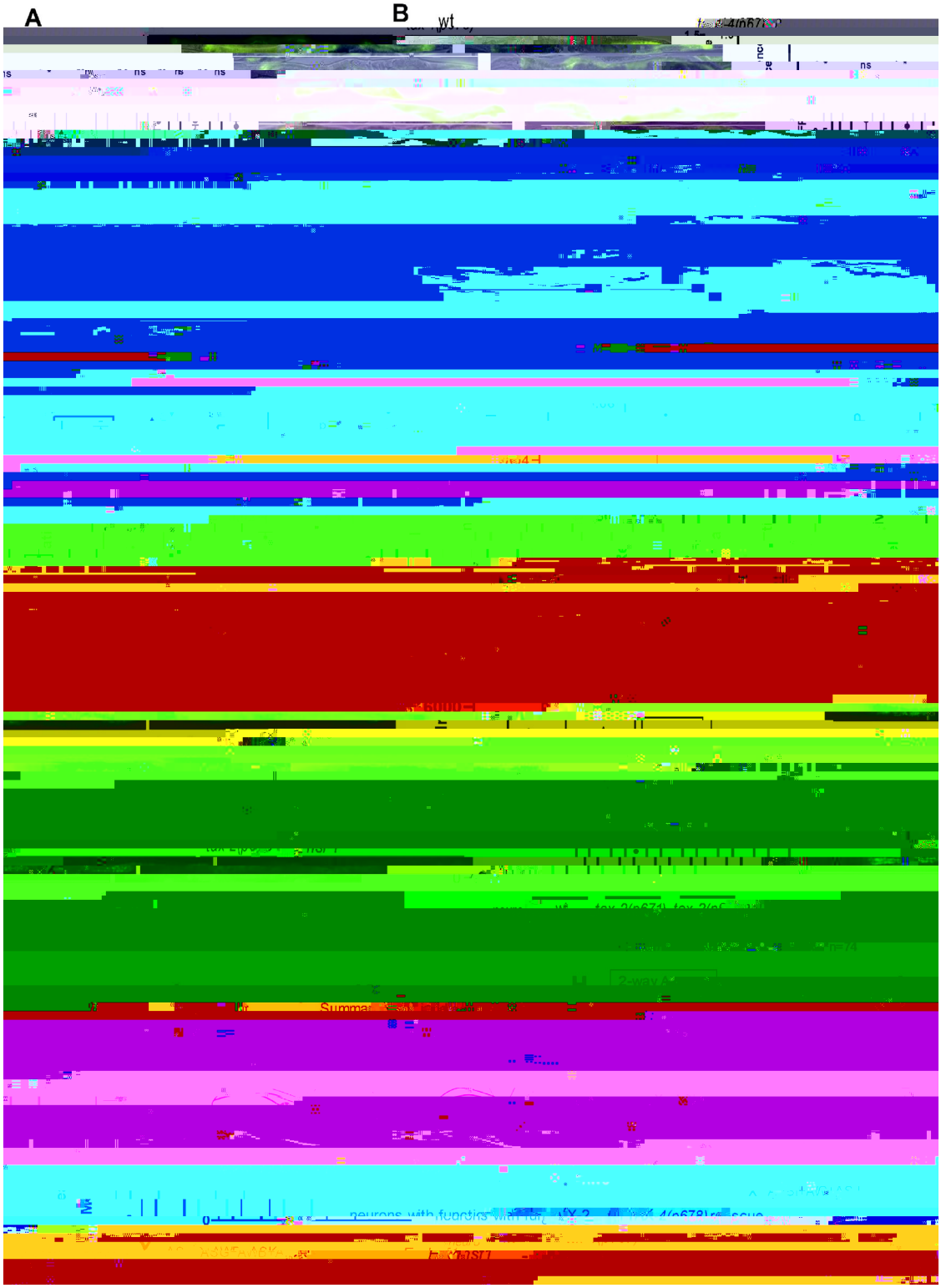

Fig 3. Neuronal cells expressing the cGMP gated cation channel TAX-2/TAX-4 are required to modulate the effect of neuronal stress on fat-remodeling in the intestine. (A) RNAi-based screen for suppressors of the repressive effect of *hsf-1*^{neuro} on *fat-7* expression (details in Methods). *Ex hsf-1*^{neuro}*; fat-7p*::*GFP; rrf-3* (MOC201) were treated with RNAi against 8 genes expressed in neuronal cells that are known or suspected to influence fat metabolism. The graph compares mean expression values of RNAi-fed *Ex hsf-1*^{neuro} (+/−) pairs, where the average mean intensity values of GFP driven by *fat-7p*::*GFP* in animals containing the *Ex hsf-1*^{neuro}

We sought to further narrow down specific TAX-2/4±expressing

2/4±expressing neurons are responsible for remodeling and that they must be required for the regulation of a neuroendocrine signal(s) in order to cause cell nonautonomous alterations in lipid metabolism.

Neuronal stress controls fat metabolism by decreasing TGF-**β**/BMP signaling

We next investigated how *hsf-1*^{neuro} activity in neurons is signaled across tissues to remodel fat metabolism. When performing an in-depth phenotypic characterization of *hsf-1*^{neuro}

Fig 4. Neuronal stress remodels fat metabolism by suppressing TGF-β/BMP signaling. (A±C) Neuronal stress decreases the fluorescent GFP output of an in vivo RAD-SMAD reporter that directly and positively responds to TGF- /BMP signaling [48]. (A) At 20ÊC, there is a reduction in nuclear GFP signal of L4.8-stage, *hsf-1*^{neuro} *#2* animals (MOC229, lower panel) compared to age-matched controls (LW2436, upper panel). (B) Quantification of fluorescence levels of RAD-SMAD reporter in large intestinal nuclei (>60 um) (C) and in small hypodermal nuclei (<60 um). Paired *t* test shows a significant difference in the mean fluorescence levels of controls relative to *hsf-1*^{neuro} *#2* animals (S6 Table). *N* values correspond to the number of fluorescent nuclei across all worms from 4 independent Paired Tdl 4u8 1 T4 ().)Tj /F98c06 0 Td (tce)Tj 3.5433

(VNC) cells Ð using *dbl-1p*::*dbl-1*::*TM*::*mcherry* [49] behaves in the same manner as the loss of *dbl-1* function for *fat-7p*::*GFP* levels or fat accumulation [13] (S5E Fig). Although these results are surprising, they suggest that the exact dose of TGF- /BMP expression is key.

Collectively, these data indicate that increased activity of *hsf-1*^{neuro} in neurons suppresses TGF- /BMP signaling, causing multiple cell nonautonomous changes including a reduction of *fat-7* expression, fat stores, and body

gfp is driven by *unc-47*, a promoter that is restricted to GABAergic neurons and that lack HSF-1 binding sites, *gfp* expression is independent of temperature (Fig 6E).

One potential scenario is that the neurons that activate the HSR at 25ÊC are TAX-2/4± expressing neurons. To determine if this was the case, we performed a co-localization experiment using 2 independent reporters (either mORANGE or wrmSCARLET driven by the *tax-4* promoter) in addition to the cGAL system to monitor neurons with an active HSR. As shown in S6A and S6B Fig, the analysis of both reporters indicates no direct co-localization between TAX-4 neurons and neurons with an active HSR. However, neuronal

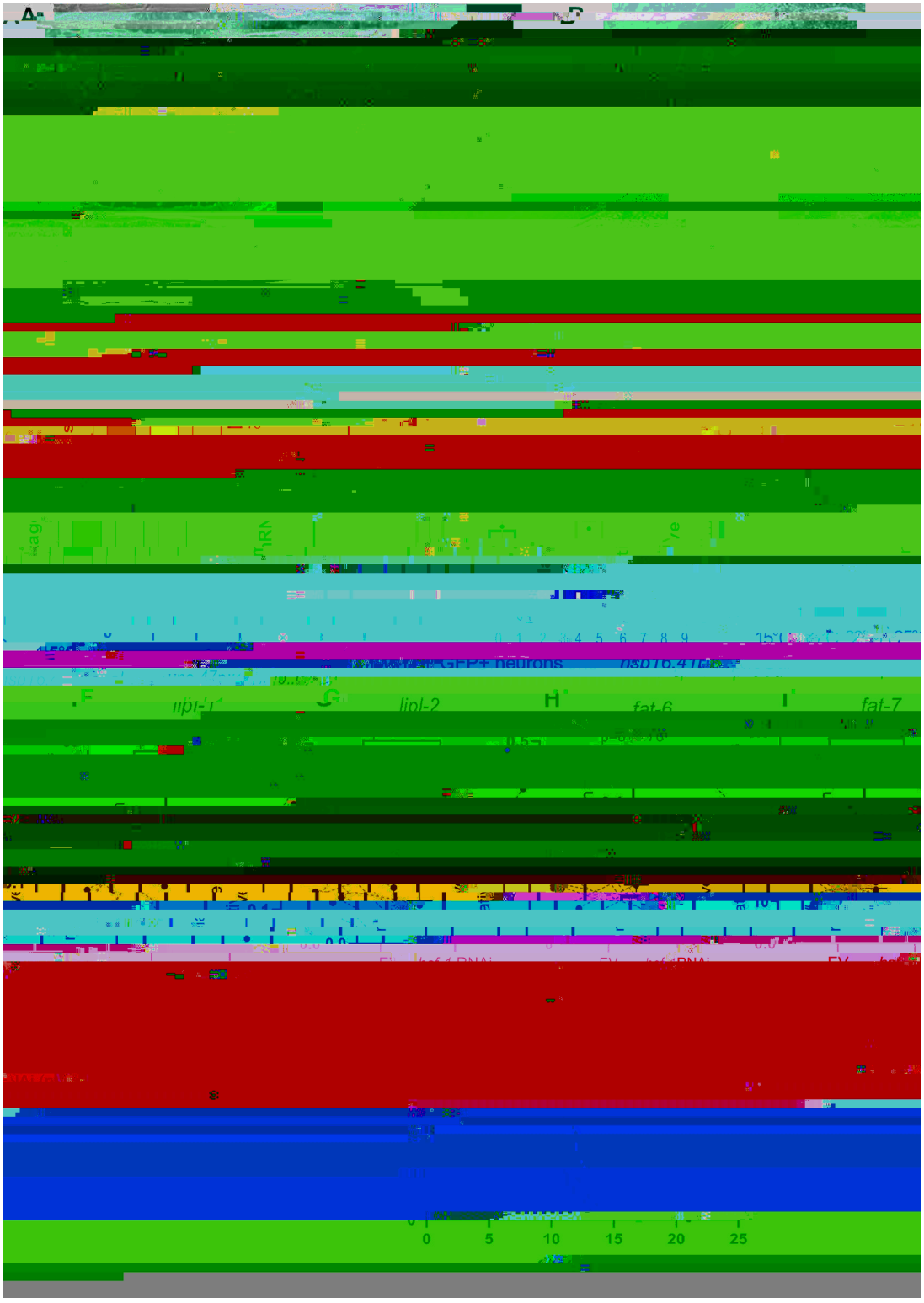

Fig 6. Evidence for an HSF-1±dependent thermostat in WT animals. (A, B) The figures show representative images taken at 20× magnification with both GFP fluorescence and Nomarski optics of young adult *hsp16.41p*:cGAL/UAS:GFP (PS7171) animals raised at 20ÊC. In the absence of stress, GFP is expressed exclusively in anterior cells and occasionally in tail neurons (arrowhead in A). The cells are neurons as they show axonal projections (in B, arrowhead points at a visible axonal projection). Animals shown were straightened using the Worm-align FIJI-based pipeline [53]. Scale bar: 100 μm (A), 50 μm (B). (C) Neuronal

the hypodermis (S8 Fig), unreported leakage to other tissues may have an influence on the Lof phenotypes observed. We have summarized the model in Fig 5.

Discussion

Our results show that the overexpression of *hsf-1* in neurons leads to LDs depletion and widespread remodeling of the abundance and composition of membrane PLs, in a manner that would support homeoviscous adaptation to high temperatures (S9 Fig). We identify 2 independent molecular pathways, the first regulates the fat desaturases *fat-6* and *fat-7*Ð with the latter normally down-regulated at 25ÊC. The data presented are consistent with the idea that overexpression of *hsf-1* in 6 or more TAX-2/4 neurons is sufficient to switch off fat desaturation by decreasing TGF- /BMP ligand availability and down-regulation of pathway component expression and activity. Additional signals are required, however, for this branch of the pathway to act under physiological conditions. The second branch is required for the up-regulation of acid lipases under warm temperatures, and it is controlled by unknown sensory neurons and signals. In the first *fat-6/7* branch, *hsf-1* expression in TAX-2/4 neurons is sufficient but not necessary to exert neuroendocrine control of fat remodeling, whereas in lipase branch, *hsf-1* is both necessary and sufficient and requires a key but indirect input from TAX-2/4 neurons (see model in Fig 5).

We currently know of 2 main strategies for dealing with temperature. Endotherms, such as mammals and avian (88ons)TjTj /F8 1 us (modell hTj /F9 1d (2)Tj 0.6973 0 Td879i796rd (signa.1849 0

function in neurons to centrally coordinate membrane composition across tissues. Endotherms have peripheral thermostat sensors that relay information to the hypothalamus. We find that in worms, a ªhypothalamus-likeº group of neurons may be both sensing environmental

MOC227 *uthIs66 [hsf-1^{neuro} line # 1(rab-3p:: hsf-1^{neuro}); myo-2p::tomato]; rtIs30 [fat-7p:: GFP]*

MOC229 *uthIs368 [hsf-1^{neuro} line#2 (rab-3p:: hsf-1^{neuro}); myo-2p::tomato]; jjIs2277 [pCXT51 (5 RLR::pes-10p(deleted)::GFP) + LiuFD61(mec-7p::RFP)] I or IV*

MOC232 *uthEx663 [Ex-hsf-1^{neuro}* (*rab-3p:: hsf-1^{neuro}); myo-2p::tdtomato]; rtIs30 [fat-7p:: GFP]; tax-4 (p678) III*

MOC235 *uthEx663 [Ex-hsf-1^{neuro}* (*rab-3p:: hsf-1^{neuro}); myo-2p::tdtomato]; rtIs30 [fat-7p:: GFP]; ttx-3(ks5) X*

MOC252 *uthIs68 [hsf-1^{neuro} line#2 (rab-3p:: hsf-1^{neuro}); myo-2p::tomato]; tax-2(p671) I*

MOC253 *uthIs368 [hsf-1^{neuro} line#2(rab-3p:: hsf-1^{neuro}); myo-2p::tomato]; tax-2(p671) I; dbl-1 (nk3) V*

MOC254 *uthIs368 [line#2 (rab-3p:: hsf-1^{neuro}); myo-2p::tomato]; dbl-1(nk3) V*

MOC279 *dbl-1(nk3)* V; *rtIs30 [fat-7p::GFP]*

MOC293 *uthIs368 [hsf-1^{neuro} line#2 (rab-3p:: hsf-1^{neuro}); myo-2p::tomato]; tax-2(p694) I*

MOC297 *uthEx663 [Ex-hsf-1^{neuro} (rab-3p:: hsf-1^{neuro}); myo-2p::tdtomato]; rtIs30 [fat-7p:: GFP]; ttx-1(p767) V*

MOC299 *uthIs368 [hsf-1^{neuro} line#2 (rab-3p:: hsf-1^{neuro}); myo-2p::tdtomato]; waEx16 [fat-6p::GFP + lin-15(+)]*

MOC312 *tax-2(p671)* outcrossed 3 times (parental strain PR671)

MOC315 *tax-4 (p678) III; rtIs30 [fat-7p::GFP]; uthEx663[rab-3p:: hsf-1$^{neuro;}$ myo-2p::tdtomato]; bicEx34 [trx-1p::tax-4cDNA; myo-3p::mcherry]*, *tax-4* rescue in ASJ, line #1.1@5

MOC316 *tax-4 (p678) III; rtIs30 [fat-7p::GFP]; uthEx663[rab-3p:: hsf-1$^{neuro;}$ myo-2p::tdtomato]; bicEx35 [trx-1p::tax-4cDNA; myo-3p::mcherry]*, *tax-4* rescue in ASJ, line #1.1

MOC322 *tax-4 (p678) III; rtIs30 [fat-7p::GFP]; uthEx663[rab-3p::; myo-2p::tdtomato]; bicEx41 [ceh-36p::tax-4cDNA; myo-3p::mcherry]*, *tax-4* rescue in AWC, line #2.3@5

MOC327 *tax-4 (p678) III; rtIs30 [fat-7p::GFP]; uthEx663[rab-3p:: hsf-1$^{neuro;}$ myo-2p::tdtomato]; bicEx46 [str-3p::tax-4cDNA; myo-3p::mcherry*], *tax-4* rescue in ASI, line #3.6@5

MOC328 *tax-4 (p678) III; rtIs30 [fat-7p::GFP]; uthEx663[rab-3p:: hsf-1$^{neuro;}$ myo-2p::tdtomato]; bicEx47 [trx-1p::tax-4cDNA; ceh-36p::tax-4cDNA; myo-3p::mcherry]*, *tax-4* rescue in ASJ+AWC, line #4.4

MOC329 *tax-4 (p678) III; rtIs30 [fat-7p::GFP]; uthEx663[rab-3p:: hsf-1$^{neuro;}$ myo-2p::tdtomato]; bicEx48 [trx-1p::tax-4cDNA; ceh-36p::tax-4cDNA; myo-3p::mcherry]*, *tax-4* rescue in ASJ+AWC, line #4.6

MOC331 *tax-4 (p678) III; rtIs30 [fat-7p::GFP]; uthEx663[rab-3p:: hsf-1$^{neuro;}$ myo-2p::tdtomato]; bicEx50 [trx-1p::tax-4cDNA; str-3p::tax-4cDNA; myo-3p::mcherry]*, tax-4 rescue in ASJ +ASI, line #5.2

MOC332 *tax-4 (p678) III; rtIs30 [fat-7p::GFP]; uthEx663[rab-3p:: hsf-1$^{neuro;}$ myo-2p::tdtomato]; bicEx51 [ceh-36p::tax-4cDNA; str-3p::tax-4cDNA; myo-3p::mcherry]*, *tax-4* rescue in AWC +ASI line #6.2

MOC333 *tax-4 (p678) III; rtIs30 [fat-7p::GFP]; uthEx663[rab-3p:: hsf-1$^{neuro;}$ myo-2p::tdtomato]; bicEx52 [trx-1p::tax-4cDNA; ceh-36p::tax-4cDNA; str-3p::tax-4cDNA; myo-3p::mcherry]*, *tax-4* rescue in ASJ +AWC +ASI, line #7.4

MOC335 *tax-4 (p678) III; rtIs30 [fat-7p::GFP]; uthEx663[rab-3p:: hsf-1$^{neuro;}$ myo-2p::tdtomato]; bicEx54 [str-3p::tax-4cDNA; myo-3p::mcherry]*, *tax-4* rescue in ASI, line #3.4@5

MOC340 *xuEx2070[Ptrx-1::TeTx::sl2::yfp; uthEx663[rab-3p:: hsf-1$^{neuro;}$ myo-2p::tdtomato]*, tetanus toxin in ASJ neuron, blocks neurotransmission from ASJ

MOC342 *peIs1715 [str-1p::mCasp-1 + unc-122p::GFP*, *uthEx663[rab-3p:: hsf-1$^{neuro;}$ myo-2p::tdtomato]*, AWB neuron eliminated

MOC343 *qrIs2 [sra-9::mCasp1] + intestinal GFP marker; uthEx663[rab-3p:: hsf-1*$^{neuro;}$ *myo-2p::tdtomato]*, ASK neuron eliminated

MOC346 *tax-4(p678) III; dbEx834[pops-1::tax-4cDNA::sl2mcherry; ccGFP]; rtIs30 [fat-7p:: GFP]; uthEx663[rab-3p:: hsf-1*$^{neuro;}$ *myo-2p::tdtomato]*, *tax-4* rescue in ASG

MOC347 *dbl-1(nk3) V; uthIs368[rab-3p:: hsf-1*$^{neuro;}$ *myo-2p::tomato]; rtIs30 [fat7p::GFP]*

MOC353 *rtIs30[fat-7p::GFP]; bicEx55 [oLC04 tax-4p::hsf-1(cDNA)::unc-54 3′ UTR; myo-2p::RFP] line 2*

MOC354 *rtIs30[fat-7p::GFP]; bicEx55 [oLC04 tax-4p::hsf-1(cDNA)::unc-54 3′ UTR; myo-2p::RFP] line 1*

MOC367 *bicEx68[tax-4p::his-24::morange (pAS1); bus-1p::GFP] syIs337 [15xUAS::?pes-10:: GFP::let-858 3′ UTR + ttx-3p::RFP + 1kb DNA ladder (NEB)] III. syIs400 [hsp16.41p::NLS:: GAL4SK::VP64::let-858 3′ UTR + unc-122p::RFP + 1kb DNA ladder (NEB)] V line 1*

MOC372 *uthIs368[rab-3p::hsf-1*^{neuro}*; myo-2p::tomato]; ctIs43[dbl-1p:;GFP;dbl-1p::GFP:: NLS]*

MOC377 *Ex[dbl-1p::dbl-1::mcherry; unc-122p::GFP]; uthEx663[rab-3p::hsf-1; myo-2p::tdto-mato]; rtIs30[fat-7p::GFP]*

MOC381 *icbEx246[pFD18(tax-4::tax-4::wrmScarlet::SL2::unc-54),pRJM163 (bus-1::GFP), BJ36]; syIs337 [15xUAS::?pes-10::GFP::let-858 3′ UTR + ttx-3p::RFP + 1kb DNA ladder(NEB)] III. syIs400 [hsp16.41p::NLS::GAL4SK::VP64::let-858 3′ UTR + unc-122p::RFP + 1kb DNA lad-der(NEB)] V*

N2 *wild type*

NL2099 *rrf-3(pk1426) II*

NU3 *dbl-1(nk3) V*

PR671 *tax-2(p671) I*

PR694 *tax-2(p694) I*

PR767 *ttx-1(p767) V*

PS6025 *qrIs2 [sra-9::mCasp1]* + intestinal GFP marker, caspase expression in ASK neuron

PS7167 *syIs396 [unc-47p::NLS::NLS::GAL4SK::VP64::let-858 3′ UTR + unc-122p::RFP + 1kb DNA ladder (NEB)]; syIs337 [15xUAS::?pes-10::GFP::let-858 3*

L1 plating at 15ÊC, 20ÊC and 25ÊC, respectively. The timing of mutant animals collected in parallel was adjusted from the WT timing, when developmental delay was noticed. For bulk quantitative RT-PCR (qRT-PCR) experiments and for microscopy-based quantification of fluorescent reporters at L4.8 or L4.9 stages, we used worms synchronized by egg laying and grown in parallel at different temperatures. Worms were harvested 97 hours after egg laying at 16ÊC, 42 hours after egg laying at 25ÊC, and L4.8 or L4.9 worms were

DNA lysate preparation and PCR genotyping

Between 10 and 100 worms were picked into 10 µL of Worm Lysis Buffer (50mM KCl, 10mM

temperature.

plasmids were injected at a lower final concentration of 5 ng/µL each plasmid to avoid potential toxicity issues. For *tax-4* expressing neurons co-localization experiments (

RNA-seq library preparation

RNA was extracted by standard Trizol extraction techniques. Libraries were made using either NEBNext mRNA Second Strand Synthesis Module (E6111) followed by NEBNext Ultra II DNA Library Prep Kit for Illumina (NEB-E7645) or NEBNext Ultra II Directional RNA Library Prep Kit for Illumina (E7760) with the NEBNext Poly(A) mRNA Magnetic Isolation Module (NE7490) as per manufacturer's protocols using half reactions. A total of 13 cycles of amplification was used for library enrichment; quality and size distribution of the libraries were ascertained by running on a Bioanalyzer High Sensitivity DNA Chip (Agilent (Santa Clara, USA), 5067±4626), and concentration was determined using KAPA Library Quantification Kit (KK4824). Libraries were sequenced on an Illumina HiSeq 2500 system by the Babraham Sequencing Facility. The experiment compared 3 independent replicates WT (N2) and *hsf-1*^{neuro} (AGD1289) animals.

Quantification and statistical analysis

Statistical analysis. Statistical information for each experiment can be found in the corresponding figure legend and was obtained with Prism 8.0.

Fluorescence quantification and worm area measurements. Fluorescence images of *fat-7p*::GFP reporter at young adult stage (Figs 2H and 4D) or day 3 adults (Fig 3J) and BODIPY fat staining images, all taken at young adult stage (Figs 2E, 2G, 3F, and 4G), were quantified using an in-house±designed semiautomated workflow [53]. In order to straighten and quantify fluorescence from acquired *C*. *elegans* images, we have developed a FIJI/ImageJ workflow called ªWorm-alignº that allows to generate single- or multichannel montage images of aligned worms from selected animals in the raw image. The output of ªWorm-alignº was then imported and run through a CellProfiler pipeline called ªWorm_CPº for fluorescence quantification of the animals of interest selected with ªWorm-align.º One output parameter of the ªWorm_CPº pipeline is the area measurement for every worm, which was used as a proxy of the size of the animals (S2A Fig). Both ªWorm-alignº and ªWorm_CPº pipelines are available and described in [53]. For images of *fat-7p*::GFP reporter taken in animals at day 3 of adulthood (Fig 3C and 3H), and of *fat-6p*::GFP fluorescence at day 3 of adulthood (Fig 2J), *fat-7*p::GFP and *fat-6p*::GFP fluorescence was quantified manually in FIJI/ImageJ by circling every worm and a dark background zone in each image. The fluorescence intensity was measured in the region of interest (ROI) manager, and the value measured for the image background was subtracted from each individual worm fluorescence measurement, as described in [74]. GFP fluorescence from Z-stack confocal images of LW2436 and MOC229 animals, carrying the nuclear RAD-SMAD reporter (Fig 4B and 4C), was quantified using Fiji software. The RAD-SMAD reporter is expressed mainly in epidermal nuclei and in large intestinal nuclei. To discriminate between both tissues, GFP fluorescence was quantified either for large nuclei (>60 μm), corresponding to intestinal nuclei, or smaller nuclei (<60 μm), corresponding to epidermal nuclei. For imaging of the ctIs43 [dbl1-pGFP + dbl-1p::NLS] transgene (S6B and S6D Fig), a minimum of 10 Z-stacks were acquired of individual worms on a Nikon Ti Eclipse inverted epifluorescence microscope (objective 20×) with a 0.8-μm step size across a 17.35-μm z-0 T 3.50 Td (dbl0 0 Td 3 03f (1 Tf 0 Td (or)Tj 1.0999 0 To)Tj 1.7large)Tj

(DOI: 10.14806/ej.17.1.200), and then mapped to the *C. elegans* reference genome WBcel235 using HISAT2 v2.1.0 [78] in either single- or paired-end mode depending on the sequencing protocol followed. To improve the mapping efficiency across splice junctions, HISAT2 took as additional input the list of WBcel235.75 known splice sites. RNA-seq QC and analysis was performed on the mapped reads using the genome browser SeqMonk v1.45.4 (https://www.
bidaTo

S8 Fig. Neuronal and not epidermis expression

Acknowledgments

We dedicate this work to the memory of Michael J.O. Wakelam.

We would like to acknowledge Michael Fasseas (Invermis, Magnitude Biosciences) for plasmid injections and Sunny Biotech for transgenics; Catalina Vallejos and John Marioni for statistical advice at the beginning of the work; Simon Walker, Imaging, Bioinformatics and Lipidomics Facilities at Babraham Institute for technical support; and Cindy Voisine, Michael Witting, Jon Houseley, Len Stephens, Carmen Nussbaum Krammer, Rebeca Aldunate, Patricija van Oosten-Hawle, Jean-Louis Bessereau, and Jane Alfred for feedback on the manuscript. We thank Andy Dillin, Atsushi Kuhara, Amy Walker, Andrew Leifer, Yun Zhang, and Michalis Barkoulas for reagents and Julie Ahringer, Anne Ferguson-Smith, and Anne Corcoran for support and helpful discussions. We also acknowledge Babraham Institute Facilities.

Contact for reagent and resource sharing

Further information and requests for resources and reagents should be directed to and will be fulfilled by the Lead Contact, Olivia Casanueva (moc771@gmail.com).

Author Contributions

Conceptualization: Laetitia Chauve, Sharlene Murdoch, Michael J. O. Wakelam, Olivia Casanueva.

Data curation: Laetitia Chauve, Francesca Hodge, Sharlene Murdoch, Andrea F. Lopez-Clavijo, Olivia Casanueva.

Formal analysis: Laetitia Chauve, Anne Segonds-Pichon, Steven W. Wingett, Olivia Casanueva.

Funding acquisition: Olivia Casanueva.

Investigation: Laetitia Chauve, Francesca Hodge, Sharlene Murdoch, Fatemeh Masoudzadeh, Harry-Jack Mann, Cheryl Li, Olivia Casanueva.

Methodology: Laetitia Chauve, Francesca Hodge, Sharlene Murdoch, Andrea F. Lopez-Clavijo, Hanneke Okkenhaug, Greg West, Bebiana C. Sousa, Hermine Kienberger, Karin Kleigrewe, Mario de Bono.

Project administration: Francesca Hodge, Sharlene Murdoch, Olivia Casanueva.

Resources: Laetitia Chauve, Olivia Casanueva.

Supervision: Laetitia Chauve, Sharlene Murdoch, Olivia Casanueva.

Validation: Olivia Casanueva.

Visualization: Laetitia Chauve, Francesca Hodge, Sharlene Murdoch, Harry-Jack Mann, Olivia Casanueva.

Writing ± original draft: Olivia Casanueva.

Writing ± review & editing: Laetitia Chauve, Olivia Casanueva.

References

1. Sulston JE. The nematode Caenorhabditis elegans. Wood WB, editor. Cold Spring Harbor Laboratory Press; 1988. p. 667.
2. Lindquist S. The Heat-Shock Response. Annu Rev Biochem. 1986; 55:1151±91. https://doi.org/10.1146/annurev.bi.55.070186.005443 PMID: 2427013